Article



# $(Ca, Eu, Yb)_{23}Cu_7Mg_4$ as a Step towards the Structural Generalization of Rare Earth-Rich Intermetallics

Pavlo Solokha , Riccardo Freccero , Serena De Negri *

Posted Date: 5 January 2024

doi: 10.20944/preprints202401.0440.v1

Keywords: Rare earh rich alloys; Mg centered core-shell polyicosahedral clusters; Linear intergrowth structures; Structural generalization

*Article*

# {Ca, Eu, Yb}$_{23}$Cu$_7$Mg$_4$ as a Step towards the Structural Generalization of Rare Earth-Rich Intermetallics

**P. Solokha, R. Freccero and S. De Negri ***

Dipartimento di Chimica e Chimica Industriale, Università degli Studi di Genova, via Dodecaneso 31, 16146 Genova, Italy

* Correspondence: author e-mail: serena.denegri@unige.it (S. De Negri)

**Abstract:** The $R_{23}Cu_7Mg_4$ ($R$ = Ca, Eu) intermetallics, studied by single crystal X-ray diffraction, were found to be isostructural with the $Yb_{23}Cu_7Mg_4$ prototype (*hP*68, $k^4h^2fca$, space group $P6_3/mmc$), forming a small group inside the bigger 23:7:4 family, otherwise adopting the *hP*68-$Pr_{23}Ir_7Mg_4$ crystal structure. The observed structural peculiarity is connected with the divalent character of the $R$ component and with a noticeable volume contraction, resulting in a clear clustering of title compounds inside the whole 23:7:4 family. The occurrence of fragments typical of similar compounds, particularly Cu-centered trigonal prisms and Mg-centered core-shell polyicosahedral clusters with $R$ at vertices, induced the search of significant structural relationships. In this work, a description of the hexagonal crystal structure of the studied compounds is proposed as a linear intergrowth along the $c$-direction of the two types of slabs $R_{10}CuMg_3$ (parent type: *hP*28-$kh^2ca$, SG 194) and $R_{13}Cu_6Mg$ (parent type: *hR*60-$b^6a^2$, SG 160). The ratio of these slabs in the studied structure is 2:2 per unit cell, corresponding to the simple equation $2\times R_{10}CuMg_3 + 2\times R_{13}Cu_6Mg = 2\times R_{23}Cu_7Mg_4$. This description assimilates the studied compounds to the $\{Ca,Eu,Yb\}_4CuMg$ ones, where the same slabs (of $p3m1$ layer symmetry) are stacked in a different way/ratio, and constitutes a further step towards a structural generalization of $R$-rich ternary intermetallics.

**Keywords::** Rare earh rich alloys; Mg centered core-shell polyicosahedral clusters; linear intergrowth structures; structural generalization

## 1. Introduction

The components interaction in $R$-$T$-$X$ intermetallic systems ($R$ = rare earth metal; $T$ = transition metal; $X$ = other metal) results in many ternary compounds with recurrent stoichiometries in different concentration ranges. These compounds have been widely studied both for their applicative and fundamental properties [1–10], and they represent an ever growing database for studying structural relationships aiming simplified descriptions and rational generalizations.

Families of rare earth-rich $R$-$T$-$X$ representatives are highly populated, especially for $R_4TX$ and $R_{23}T_7X_4$ stoichiometries, each characterized by two different crystal structures (see Figure 1).

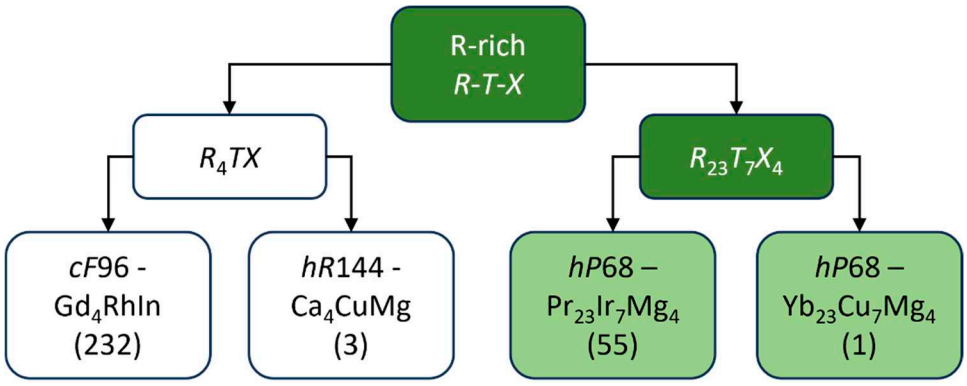

Preprints (www.preprints.org) | NOT PEER-REVIEWED | Posted: 5 January 2024 doi:10.20944/preprints202401.0440.v1



**Figure 1.** Crystal structures of the two most populated families of R-rich R-T-X intermetallics. Numbers of representatives are indicated in parentheses [8]. Green background highlights the object of current investigation.

In the framework of a recent investigation on the $R_4TX$ family, the new {Ca,Eu,Yb}$_4$CuMg compounds (*hR*144) were discovered and structurally elucidated in terms of intergrowth concept [11].

As a logical evolution of this research, our attention focused on the $R_{23}T_7X_4$ family, mostly showing the *hP*68-$Pr_{23}Ir_7Mg_4$ structure; an overview of chemical compositions of the known so far members is presented in Figure 2. This periodic table map shows that the components of these phases are light trivalent rare earth metals (*R* with Z < 65), late transition elements from 8 to 10 group (*T*) and Mg, Zn, Cd or In (*X*). As derives from the expanded table in Figure2b, the Mg and Cd containing groups are the most abundant, Zn and In having only one representative each, in combination with Ce and Ru.

The *hP*68-$Yb_{23}Cu_7Mg_4$ structure is only represented by the prototype [12], thus it was decided to perform some explorative syntheses on divalent *R* analogues (*R* = Ca, Eu) with the aim to enrich this family and looking for meaningful structural and chemical generalization criteria.

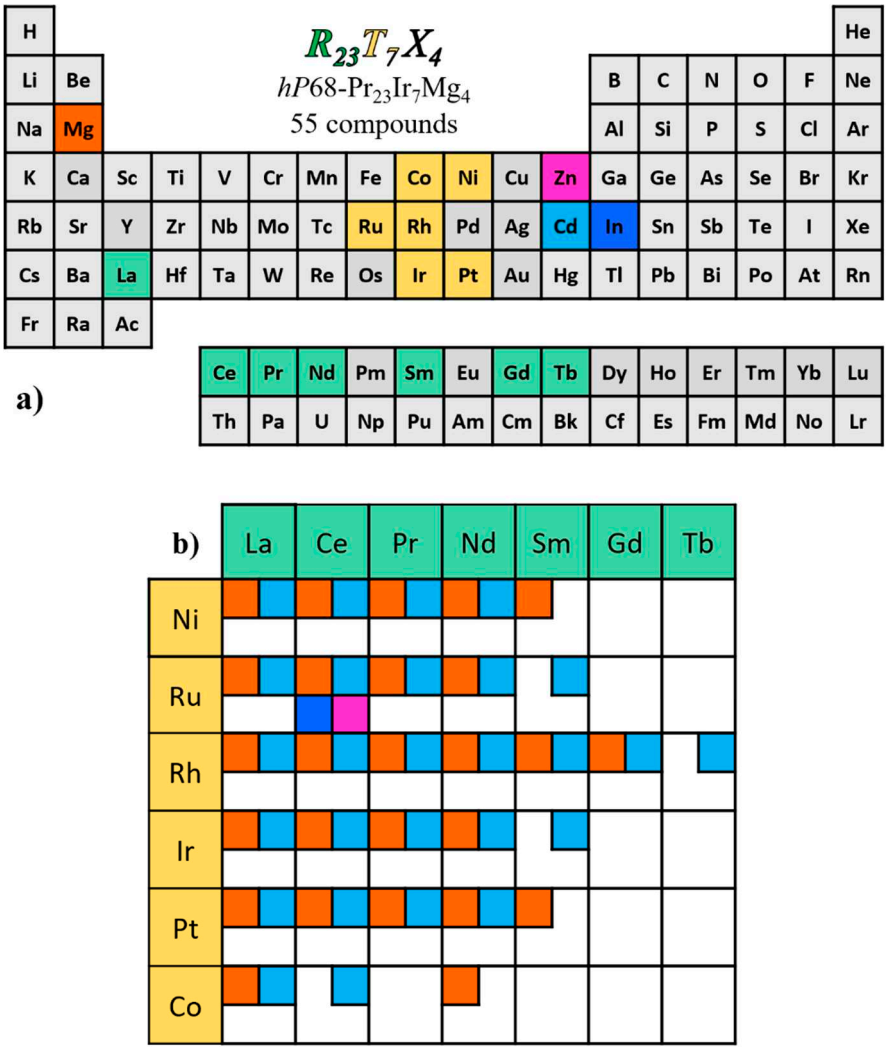


**Figure 2.** Constituents distribution among the $R_{23}T_7X_4$ family of compounds (hP68-$Pr_{23}Ir_7Mg_4$): a) elements involved mapped on a periodic table; b) expanded table representing specific ternary combinations. The colouring scheme is the same for both tables.

Preprints (www.preprints.org) | NOT PEER-REVIEWED | Posted: 5 January 2024 doi:10.20944/preprints202401.0440.v1



## 2. Experimental Section

Samples of nominal composition $Ca_{67.6}Cu_{20.6}Mg_{11.8}$ (total mass = 0.5 g) and $Eu_{66.7}Cu_{20.3}Mg_{13}$ (total mass = 0.8 g) were prepared from pure (>99.9 mass %) components. The starting metals were weighted in stoichiometric amounts and placed in tantalum crucibles, arc-sealing their cap to prevent Mg evaporation. These operations were done in a glove box filled with Ar, to minimize side reactions with oxygen and water. The Ta crucibles were put in a quartz glass tube sealed under an inert atmosphere, then placed in a resistance furnace where the following thermal cycle was applied: 20 °C → (5 °C/min) → 850 °C (10 min) → (-0.1 °C/min) → 400 °C (5 min) → (-0.2 °C/min) → 100 °C (furnace switched off).

For microscopic characterization, some pieces of each sample were selected and embedded in a conductive phenolic resin, polymerized in a hot mounting press machine Opal 410 (ATM GmbH, Germany). Surfaces were smoothed by SiC abrasive papers with no lubricant and polished with the aid of diamond pastes with particle size decreasing from 6 to 1 μm, using petroleum ether as lubricant. An automatic polishing machine Saphir 520 (ATM GmbH, Germany) was applied for this purpose.

Microstructure observation together with qualitative and quantitative analyses were conducted on a Zeiss Evo 40 Scanning Electron Microscope (SEM) equipped with a Dispersive X-ray Spectroscopy (EDXS) system (INCA X-ACT) managed by the INCA Energy software (Oxford Instruments, Analytical Ltd., Bucks, U.K.). Both samples showed a good yield of the compound of interest, of average composition ~ 67 at.% *R*, 20 at.% Cu, 13 at.% Mg (see Figure 3), and were therefore subjected to X-ray diffraction studies. X-ray Powder Diffraction (XRPD) patterns were recorded on a Philips X'Pert MPD diffractometer (Cu $K_\alpha$ radiation, step mode of scanning) and indexed by Powder Cell [13] software.

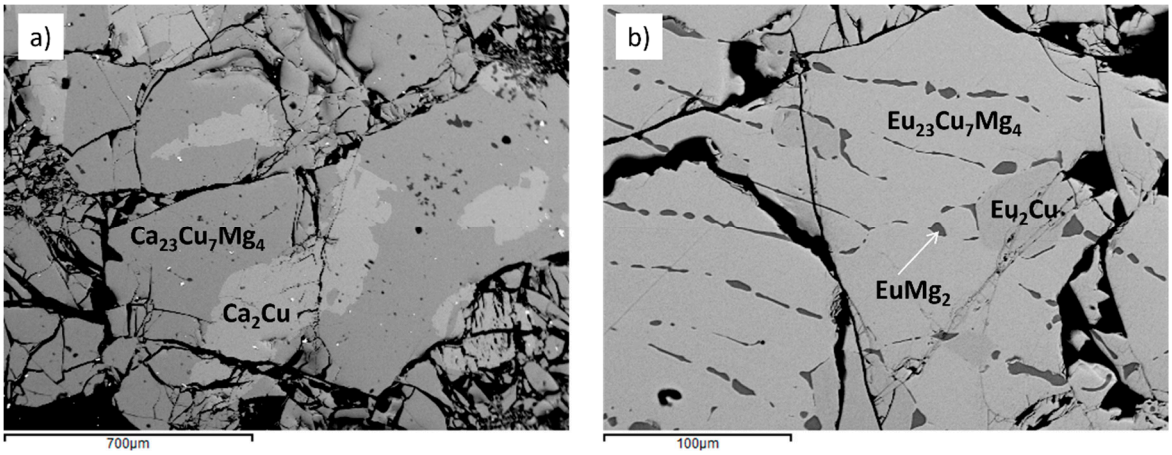


**Figure 3.** SEM images (BSE mode) of Ca-Cu-Mg (a) and Eu-Cu-Mg (b) samples. The phases detected by EDXS analysis are indicated.

Good quality single crystals were selected with the help of a light microscope from mechanically crushed alloys covered with mineral oil. Crystals, embedded in an excess of grease to prevent oxidation, were then glued to pins and remained stable for several days.

The X-ray diffraction data were collected on a three-circle Bruker D8 QUEST diffractometer equipped by a PHOTON III 14 photon counting detector, using the graphite monochromatized Mo Kα radiation. Data collection strategies, consisting of both ω- and φ-scans, were decided using the APEX4 software [14] to obtain good data completeness, redundancy, and resolution limit. Data were collected over the reciprocal space up to ~ 31° in θ (resolution of *ca.* 0.7 Å) with exposures of 30-40 s per frame. The software SAINT [15] and XPREP [16] were used for data reduction. Lorentz, polarization, and absorption effects were corrected by SADABS [17]; the crystal structure was solved and refined with the aid of SHELXTL [18].

Preprints (www.preprints.org) | NOT PEER-REVIEWED | Posted: 5 January 2024 doi:10.20944/preprints202401.0440.v1



Both crystals possess hexagonal symmetry, and their diffraction patterns show systematic absences due to the presence of a *c*-type glide plane. Reconstructed intensity profiles of selected zones are shown in Figure 4 for the Eu-compound diffraction pattern.

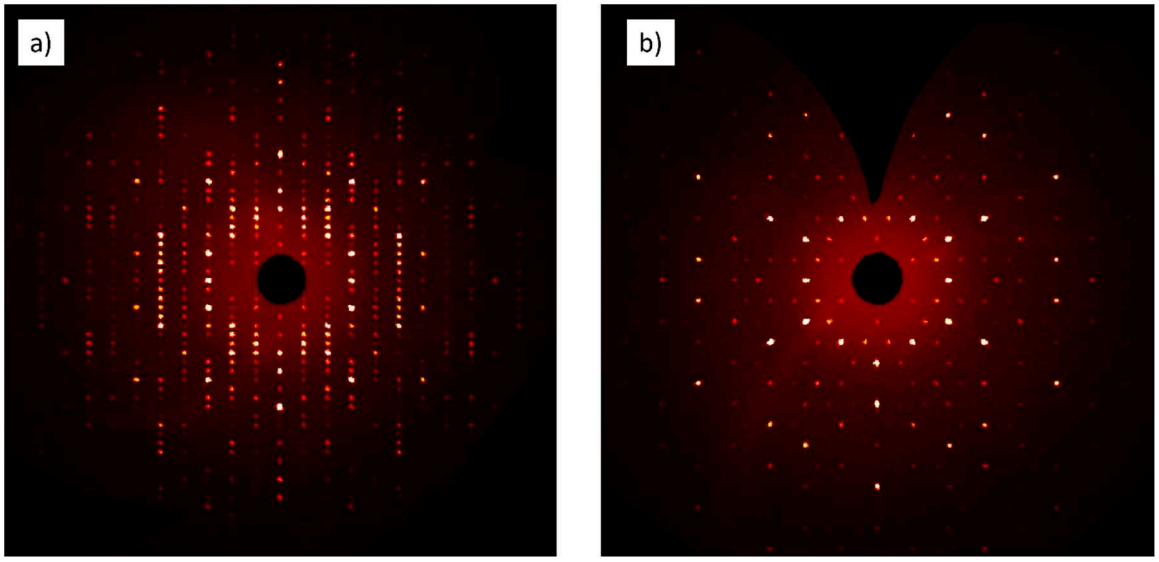


**Figure 4.** Reconstructed precession images of h0l (a) and hk0 (b) zones for the $Eu_{23}Cu_7Mg_4$.

The best structural model was found using the intrinsic phasing method in the $P6_3/mmc$ space group (N. 194), corresponding to the *hP*68-$Yb_{23}Cu_7Mg_4$ prototype. The unit cell, containing 2 formula units of $R_{23}Cu_7Mg_4$ composition, accounts for 68 atoms, distributed among 5 Wyckoff sites of *R*, 2 sites of Cu and 2 of Mg. In the case of $Ca_{23}Cu_7Mg_4$, the first refinement resulted in somewhat high isotropic displacement parameters for Mg atoms in the 2*a* position. A Mg/Ca statistical mixture was refined for this site, resulting in 0.93/0.07 ratio and significantly improving the structural model. For the Eu representative, no need of statistical mixture was evidenced, and the structural model turns out to be perfectly stoichiometric. The final anisotropic full-matrix least-squares refinements converged to good residuals for both compounds. Details of data collection and structure refinement are summarized in Table 1 together with selected crystal data; standardized atomic coordinates, site occupancy factors and equivalent displacement parameters are listed in Table 1. The corresponding CIF files, available as supplementary material, were deposited at the Cambridge Database.

**Table 1.** Selected crystallographic data and structure refinement parameters for the single crystals studied in this work.

| Formula | $Ca_{22.93(4)}Cu_7Mg_{4.07(4)}$ | $Eu_{23}Cu_7Mg_4$ |
|---|---|---|
| EDXS composition | $Ca_{68.2}Cu_{19.8}Mg_{12.0}$ | $Eu_{66.2}Cu_{19.2}Mg_{14.6}$ |
| Depositing CSD-code | 2266948 | 2266951 |
| Formula weight (g/mol) | 1463.86 | 4037.10 |
| Space group | $P6_3/mmc$ (194) | |
| Pearson symbol-protoype, Z | *hP*68-$Yb_{23}Cu_7Mg_4$, 2 | |
| *a*, Å | 10.236(2) | 10.659(2) |
| *c*, Å | 23.413(5) | 24.379(5) |
| *V*, Å$^3$ | 2124.5(9) | 2398.7(10) |
| Calc. density (g·cm$^{-3}$) | 2.29 | 5.59 |
| Absorption coefficient (μ, mm$^{-1}$) | 6.27 | 32.61 |
| Theta range (°) | $2.3 \leq \theta \leq 33.2$ | $2.8 \leq \theta \leq 30.5$ |

Preprints (www.preprints.org) | NOT PEER-REVIEWED | Posted: 5 January 2024 doi:10.20944/preprints202401.0440.v1



| | | |
|---|---|---|
| Index ranges $h$, $k$, $l$ | $-15 \le h \le 11$<br>$-15 \le k \le 14$<br>$-36 \le l \le 35$ | $-15 \le h \le 15$<br>$-15 \le k \le 13$<br>$-34 \le l \le 34$ |
| Data/parameters | 1592/41 | 1435/40 |
| *GOF* | 1.16 | 0.98 |
| $R_{int}/R_{sym}$ | 0.1014/0.045 | 0.083/0.018 |
| $R1/wR2$ ($I > 2\sigma(I)$) | 0.0403/0.0932 | 0.0259/0.0454 |
| $R1/wR2$ (all data) | 0.0864/0.1320 | 0.0445/0.0524 |
| Max diff. peak and hole ($e^-/Å^3$) | 1.19 and -1.40 | 2.59 and -1.36 |

## 3. Results and Discussion

The studied $\{Ca,Eu\}_{23}Cu_7Mg_4$ compounds, together with the Yb-containing prototype, form a small sub-family of $R_{23}T_7X_4$ with crystal structure (*hP*68-$Yb_{23}Cu_7Mg_4$, Wyckoff sequence $k^4h^2fca$, see Table 2) different from all the others (*hP*68-$Pr_{23}Ir_7Mg_4$, Wyckoff sequence $c^{10}b^2a^2$), however having in common with them the hexagonal symmetry and the number of atoms in the unit cell.

**Table 2.** Standardized atomic coordinates and equivalent displacement parameters ($U_{eq}$) for the $\{Ca,Eu\}_{23}Cu_7Mg_4$ single crystals.

| Atom | Site | Atomic coordinates | | | $U_{eq}$ [Å²] |
|---|---|---|---|---|---|
| | | *x*/*a* | *y*/*b* | *z*/*c* | |
| $Ca_{22.93(4)}Cu_7Mg_{4.07(4)}$ | | | | | |
| Ca1 | 4*f* | 1/3 | 2/3 | 0.61757(8) | 0.0180(4) |
| Ca2 | 12*k* | 0.20651(6) | 0.4130(1) | 0.03215(5) | 0.0209(2) |
| Ca3 | 6*h* | 0.12164(9) | 0.24328(9) | 1/4 | 0.0211(3) |
| Ca4 | 12*k* | 0.12389(6) | 0.2478(1) | 0.61877(5) | 0.0219(2) |
| Ca5 | 12*k* | 0.53951(6) | 0.07902(6) | 0.66824(5) | 0.0217(2) |
| Cu1 | 12*k* | 0.52555(4) | 0.05110(4) | 0.04959(3) | 0.0243(2) |
| Cu2 | 2*c* | 1/3 | 2/3 | 1/4 | 0.0277(4) |
| Mg1 (Ca)<br>SOF(Mg) = 0.93 | 2*a* | 0 | 0 | 0 | 0.0234(17 |
| Mg2 | 6*h* | 0.7706(1) | 0.5412(3) | 1/4 | 0.0190(5) |
| $Eu_{23}Cu_7Mg_4$ | | | | | |
| Eu1 | 4*f* | 1/3 | 2/3 | 0.61610(3) | 0.0221(2) |
| Eu2 | 12*k* | 0.20717(3) | 0.41434(5) | 0.03062(2) | 0.0244(1) |
| Eu3 | 6*h* | 0.12316(4) | 0.24632(4) | 1/4 | 0.0264(1) |
| Eu4 | 12*k* | 0.12549(3) | 0.25099(5) | 0.61768(2) | 0.0277(1) |
| Eu5 | 12*k* | 0.53839(2) | 0.07678(2) | 0.66768(2) | 0.0240(1) |
| Cu1 | 12*k* | 0.52492(6) | 0.04984(4) | 0.04907(6) | 0.0308(3) |
| Cu2 | 2*c* | 1/3 | 2/3 | 1/4 | 0.0311(6) |
| Mg1 | 2*a* | 0 | 0 | 0 | 0.0255(6) |
| Mg2 | 6*h* | 0.76850(2) | 0.53700(5) | 1/4 | 0.0254(9) |

Preprints (www.preprints.org) | NOT PEER-REVIEWED | Posted: 5 January 2024 doi:10.20944/preprints202401.0440.v1



A first glance to the crystal structures of interest in terms of interatomic distances shows that the *R*–Mg (3.52 ÷ 3.74 Å for Ca, 3.69 ÷ 3.90 Å for Eu), Cu–Cu (2.49 for Ca, 2.56 for Eu) and Mg–Mg (3.19 for Ca, 3.26 for Eu) contacts are compatible with the metallic radii sums [19], instead Mg and Cu are well apart and do not interact. Also, the first coordination spheres of the different species are geometrically similar to those in other *R*-*T*-*X* compounds rich in *R*. These polyhedra are: capped Cu-centered trigonal prisms, either isolated (Cu@*R*(6+3)) or sharing a rectangular face (Cu@Cu*R*(6+2)), isolated Mg-centered icosahedra (Mg@*R*12) and polyicosahedral Mg3@*R*20 core-shell clusters (see Figure 5).

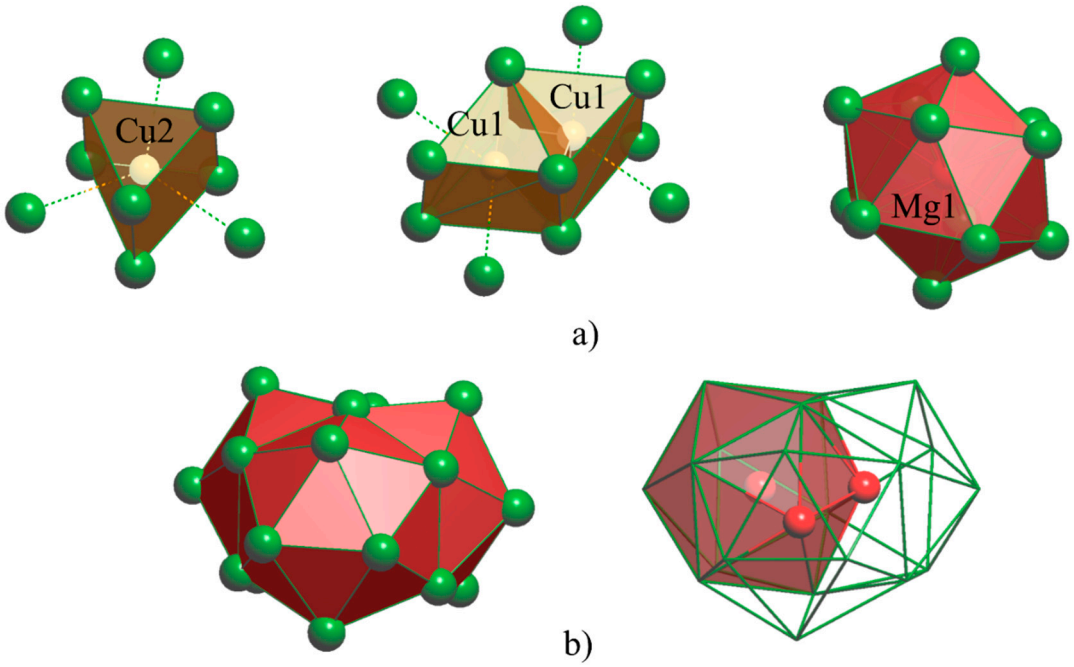


**Figure 5.** Characteristic structural fragments of {Ca, Eu, Yb}$_{23}$Cu$_7$Mg$_4$ compounds. a) coordination polyhedra for Cu and Mg1 species; b) Mg3@R20 polyicosahedral cluster (Mg2 species) with closed (left) and open/transparent (right) faces.

The same coordination polyhedra were observed in *R*$_4$CuMg (*R*=Ca, Eu, Yb) compounds [11], with a difference in the Mg-centered polyicosahedral units: in the 23:7:4 these are formed by three fused icosahedra, instead in the 4:1:1 six fused icosahedra form core-shell clusters of Mg7@*R*32 composition. Recently, we proposed an elegant description of the *R*$_4$CuMg structure in terms of linear intergrowth of slabs of *R*$_{9.5}$CuMg$_{3.5}$ and *R*$_{13}$Cu$_6$Mg composition [11]. Considering the cited similarities, an analogous description was attempted with success also for *R*$_{23}$Cu$_7$Mg$_4$ with divalent *R*.

In fact, the structure of title compounds can be interpreted as a stacking of slabs from the same parent structures, that have been extensively described in [11]: the hexagonal *hP*28-*kh*$^2$*ca* (SG 194) adopted by many *R*$_9$*TX*$_4$ and *R*$_{10}$*TX*$_3$ compounds and the rhombohedral *hR*60-*b*$^6$*a*$^2$ (SG 160) only adopted by Lu$_{13}$Ni$_6$In [20]. Slabs of each parent type are alternatively stacked along the *c*-direction, fulfilling the crystal space with no gaps neither need of "gluing" atoms (see Figure 6a). Slabs, possessing the same *p*3*m*1 layer symmetry, are joined by a common corrugated layer composed exclusively by *R* atoms, showing two types of nodes represented by (3$^6$)$^1$;(3$^2$434)$^6$ Schläfli notation (see Figure 6b).

As a consequence of this, the composition of slabs from the hexagonal parent type is *R*$_{10}$CuMg$_3$, instead the composition of other slabs is exactly *R*$_{13}$Cu$_6$Mg. Therefore, the 23:7:4 unit cell content can be easily described by properly considering the composition and number of stacked slabs: 2×*R*$_{10}$CuMg$_3$ + 2×*R*$_{13}$Cu$_6$Mg = 2×*R*$_{23}$Cu$_7$Mg$_4$.

Preprints (www.preprints.org) | NOT PEER-REVIEWED | Posted: 5 January 2024 doi:10.20944/preprints202401.0440.v1



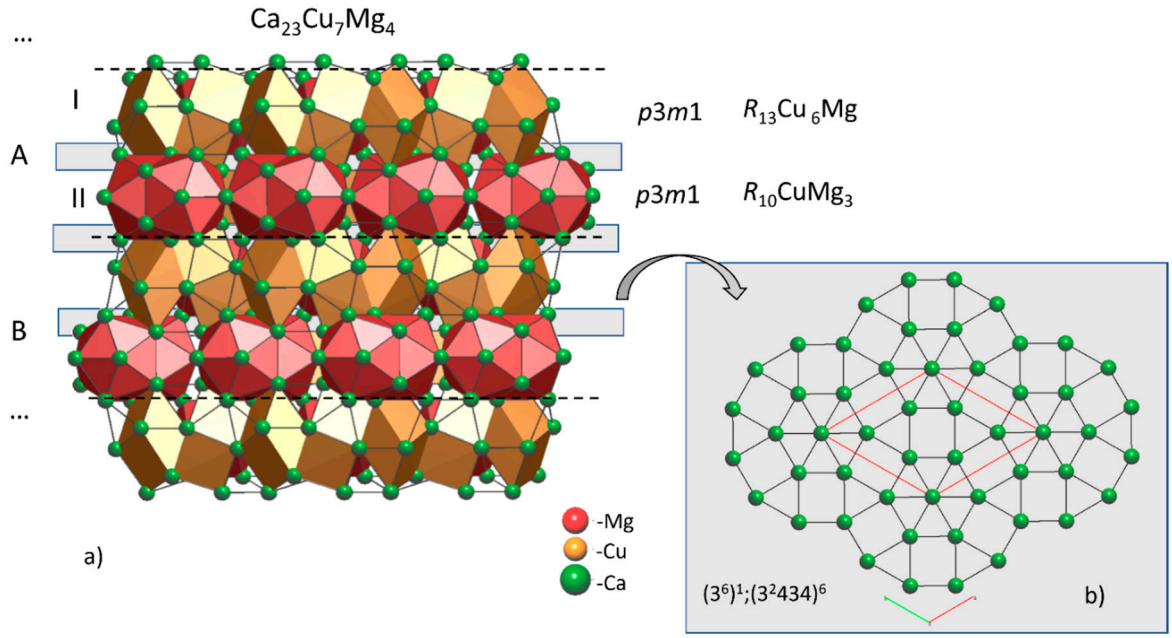


**Figure 6.** a) Crystal structure of the $Ca_{23}Cu_7Mg_4$ as a …ABAB... sequence of identical double slabs each composed of one $Ca_{13}Cu_6Mg$ (I) and one $Ca_{10}CuMg_3$ (II) single slab. The layer group symbol and thickness of each slab are indicated as well; b) top view of a sewing layer with the corresponding Schläfli notation; red lines highlight the unit cell.

It should be noted that the *P*6$_3$/*mmc* space group of title compounds is the only centrosymmetric one among the three hexagonal space groups compatible with the *p*3*m*1 layer symmetry of the stacked slabs [11]. Lattice parameters of representatives with the same slabs stacked along *c* should be related to those of the parent structures, with *a* and *b* being similar or integer multiples and *c* correlated to the total number of slabs in the unit cell: this is true for 23:7:4 and 4:1:1 compounds, having $a = b \approx 10$ Å and $c \approx 24$ Å and 51 Å, respectively.

The compositions of the two families of divalent *R*-rich compounds can be plotted on a Gibbs triangle highlighting the relation with compositions of parent types (see Figure 7) and helping to develop the structural/compositional generalization idea: in fact, hypothetic new compounds with similar intergrowth architectures should show stoichiometries laying along the dotted tie-lines.

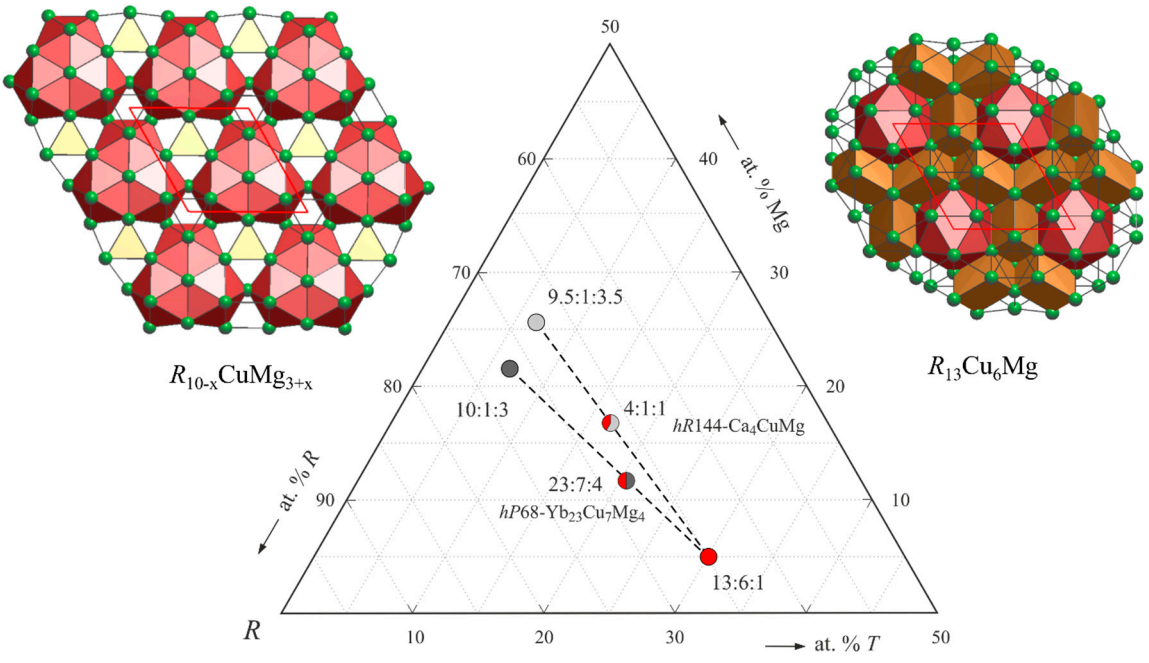

Preprints (www.preprints.org) | NOT PEER-REVIEWED | Posted: 5 January 2024 doi:10.20944/preprints202401.0440.v1



**Figure 7.** $R_4CuMg$ and $R_{23}Cu_7Mg_4$ (R = Ca, Eu, Yb) compounds represented on a partial Gibbs triangle as combinations of stoichiometries corresponding to parent types (ends of dotted segments). The specific compositions of the $R_{10-x}CuMg_{3+x}$ end member are indicated with different grey shadows. The amounts of end members in compounds of interest correspond to coloured areas ratios within the circles. Top views of the unique parent types slabs are shown as well.

At this point, it is interesting to compare the two structural sub-families of $R_{23}T_7X_4$ intermetallics in terms of their component nature. A similar analysis was applied to $R_4TMg$ using the volume contraction as a criterion. This is defined as $\Delta V_f(\%) = 100 \times \frac{V_{meas} - V_{calc}}{V_{calc}}$, where $V_{calc} = \sum_i N_i \times V_i$, ($N_i$ = number of $i$-type atoms in the unit cell, $V_i$ = atomic volume of the $i$-type species taken from [21]) and $V_{meas}$ is the experimentally determined volume [22]. Values of $\Delta V_f$ (%) for $R_{23}T_7X_4$ are plotted in Figure 8, as a function of the $T$ group and of the $R$ trivalent/divalent nature.

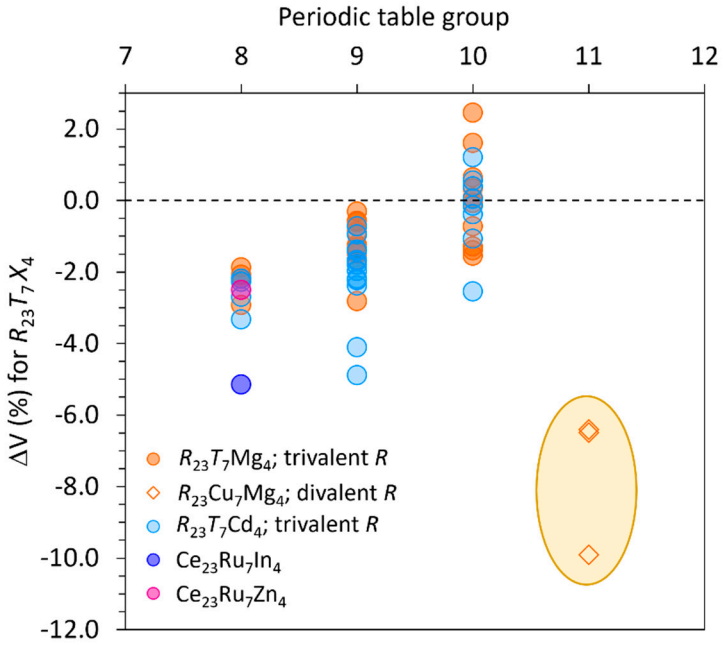


**Figure 8.** $\Delta V_f$ (%) for $R_{23}T_7X_4$ compounds. The dotted black line is an eye guide for the ideal Vegard's law behaviour. A clear separation is visible between hP68-$Pr_{23}Ir_7Mg_4$ and hP68-$Yb_{23}Cu_7Mg_4$ families of compounds.

A major part of $\Delta V_f$ (%) are negative, except for compounds with $T$ = Pt, for which values lay in the range between 0 and +2.4%. No separation is observed as a function of $X$ nature.

Instead, the title compounds, the only representatives known for divalent $R$, form a clearly clustered group, showing the most prominent volume contractions, extending down to -10% and indicating strong chemical interactions.

It is worth to note that both $R$ and $T$ nature are determinant for the formation and structure of these $R$-rich compounds; for example, the existence of $R_{23}T_7Mg_4$ has been excluded for several combinations of trivalent $R$ with {Cu, Ag, Au}[4,23–25]. On the other hand, for $T$ belonging to the 10th group no representatives were found with divalent $R$ so far: considering the similar trend observed for the structurally related 4:1:1, these combinations are indeed worth to be investigated.

## 4. Conclusions

In this work, the crystal structures of the $\{Ca,Eu\}_{23}Cu_7Mg_4$ compounds were solved by single crystal X-ray measurements, being the second and third representatives of the $Yb_{23}Cu_7Mg_4$ prototype, and forming a small structural sub-family of 23:7:4 with a divalent $R$ constituent. These few compounds are characterized by pronounced volume contractions if compared with the highly

populated $R_{23}T_7X_4$ family with trivalent *R* having $Pr_{23}Ir_7Mg_4$-type structure. The distribution of members of both groups discovered so far as a function of the nature of components suggests combinations for new exploratory syntheses aiming to enrich the $Yb_{23}Cu_7Mg_4$-type representatives, for example $R_{23}\{Ag,Au\}_7Mg_4$, $R_{23}\{Ni,Pd,Pt\}_7Mg_4$ and $R_{23}Cu_7\{Zn,Cd,Al,In\}_4$ with *R*= Ca, Eu, Yb.

The crystal structure of the title compounds was interpreted in terms of linear intergrowth of slabs $R_{10}CuMg_3$ (parent type: *hP*28-$kh^2ca$, SG 194) and $R_{13}Cu_6Mg$ (parent type: *hR*60-$b^6a^2$, SG 160), alternating along *c*-axis in the 1:1 ratio. This description brings together $\{Ca,Eu,Yb\}_{23}Cu_7Mg_4$ and $\{Ca,Eu,Yb\}_4CuMg$ compounds, the latter being formed by the same type of slabs in a 2:1 ratio. An evolution of this idea pushes towards the recognition/discovery of new structural families based on different intergrowths of the same slabs. To this purpose, the following conditions should be fulfilled:

(1) Composition restraint – stoichiometries laying along the lines joining the end-members
(2) Symmetry restraint – rhombohedral, hexagonal and cubic space groups including the *p*3*m*1 among possible s**d** linear orbits [11,26]
(3) Metric restraint – for hexagonal and rhombohedral representatives $a=b\approx10\div11$ Å or their multiples

The results of structural/chemical analysis illustrated here constitute a further step towards a planned wider generalization aimed to a simple and chemically significant representation in terms of few common building blocks of complex *R*-rich ternary intermetallics.

**Supporting Information Available** X-ray crystallographic files in CIF format.

**Conflicts of Interest** There are no conflicts to declare.

## References


1. P. Solokha, S. De Negri, V. Pavlyuk, A. Saccone, Anti-Mackay polyicosahedral clusters in La-Ni-Mg ternary compounds: Synthesis and crystal structure of the $La_{43}Ni_{17}Mg_5$new intermetallic phase, Inorg. Chem. 48 (2009) 11586–11593. https://doi.org/10.1021/ic901422v.
2. P. Solokha, S. De Negri, V. Pavlyuk, A. Saccone, The novel intermetallic phases TbNiMg and $Tb_{4+x}Ni_2Mg_{3-x}$ (x = 0.2): Synthesis, crystal structure and peculiarities, Intermetallics. 18 (2010) 719–724. https://doi.org/10.1016/j.intermet.2009.11.012.
3. P. Solokha, P.F. Rogl, A. Saccone, G. Giester, H. Michor, S. De Negri, V. Romaka, $Yb_{9+x}CuMg_{4-x}$(x = 0.034): A κ-Phase Formed by Lanthanoids, Inorg. Chem. 55 (2016) 8174–8183. https://doi.org/10.1021/acs.inorgchem.6b01315.
4. R. Freccero, S. De Negri, A. Saccone, P. Solokha, Solid state interactions in the La-Au-Mg system: phase equilibria, novel compounds and chemical bonding, Dalt. Trans. 49 (2020) 12056–12067. https://doi.org/10.1039/d0dt02359k.
5. M. Giovannini, I. Čurlík, R. Freccero, P. Solokha, M. Reiffers, J. Sereni, Crystal Structure and Magnetism of Noncentrosymmetric $Eu_2Pd_2Sn$, Inorg. Chem. 60 (2021) 8085–8092. https://doi.org/10.1021/acs.inorgchem.1c00678.
6. T. Block, S. Stein, L. Heletta, R. Pöttgen, Osmium and magnesium: Structural segregation in the rare earth-rich intermetallics $RE_4OsMg$ (RE=La-Nd, Sm) and $RE_9TMg_4$ (RE=Gd, Tb), Zeitschrift Fur Naturforsch. - Sect. B J. Chem. Sci. 74 (2019) 519–525. https://doi.org/10.1515/znb-2019-0070.
7. W. Steurer, J. Dshemuchadse, Intermetallics : structures, properties, and statistics, Oxford Univ. Press, 2016.
8. P. Villars, K. Cenzual, Pearson's Crystal Data: Crystal Structure Database for Inorganic Compounds, release 2022/2023.
9. S.J.B. Bin, K.S. Fong, B.W. Chua, M. Gupta, Mg-based bulk metallic glasses: A review of recent developments, J. Magnes. Alloy. 10 (2022) 899–914. https://doi.org/10.1016/J.JMA.2021.10.010.
10. Q. Luo, Q.F. Gu, J.Y. Zhang, S.L. Chen, K.C. Chou, Q. Li, Phase Equilibria, Crystal Structure and Hydriding/Dehydriding Mechanism of $Nd_4Mg_{80}Ni_8$ Compound, Sci. Reports 2015 51. 5 (2015) 1–14. https://doi.org/10.1038/srep15385.
11. P. Solokha, R. Freccero, S. De Negri, Architecture of new $\{Ca, Eu, Yb\}_4CuMg$ complex intermetallics based on polyicosahedral clusters, J. Solid State Chem. 328 (2023) 124353. https://doi.org/10.1016/J.JSSC.2023.124353.

12. S. De Negri, A. Saccone, P. Rogl, G. Giester, The ternary system Yb–Cu–Mg: Isothermal section at 400 °C in the range from 0 to 67 at.% Cu, Intermetallics. 16 (2008) 1285–1291. https://doi.org/10.1016/J.INTERMET.2008.08.004.
13. W. Kraus, G. Nolze, POWDER CELL-a program for the representation and manipulation of crystal structures and calculation of the resulting X-ray powder patterns, J. Appl. Cryst. 29 (1996) 301–303.
14. Bruker, APEX4 v2022.10-0, (2022).
15. Bruker, SAINT v8.30A, (2012).
16. Bruker, XPREP v2014/2, (2014).
17. Bruker, SADABS v2016/2, (2016).
18. G.M. Sheldrick, SHELXL-2019/1, (2019).
19. J. Emsley, The elements, Clarendon Press, 1998.
20. Y. V. Galadzhun, R.D. Hoffmann, L. Heletta, M. Horiacha, R. Pöttgen, The Lutetium-rich Indide $Lu_{13}Ni_6In$, Zeitschrift Für Anorg. Und Allg. Chemie. 644 (2018) 1513–1518. https://doi.org/10.1002/ZAAC.201800188.
21. P. Villars, J.L.C. Daams, Atomic-environment classification of the chemical elements, J. Alloys Compd. 197 (1993) 177–196. https://doi.org/10.1016/0925-8388(93)90041-K.
22. F. Merlo, M.L. Fornasini, Volume effects in rare earth intermetallic compounds, J. Alloys Compd. 197 (1993) 213–216. https://doi.org/10.1016/0925-8388(93)90043-M.
23. S. De Negri, M. Giovannini, A. Saccone, Constitutional properties of the La–Cu–Mg system at 400 °C, J. Alloys Compd. 427 (2007) 134–141. https://doi.org/10.1016/J.JALLCOM.2006.02.062.
24. S. De Negri, P. Solokha, A. Saccone, V. Pavlyuk, The Y-Cu-Mg system in the 0-66.7 at.% Cu concentration range: The isothermal section at 400 °C, Intermetallics. 17 (2009) 614–621. https://doi.org/10.1016/j.intermet.2009.02.001.
25. S. De Negri, P. Solokha, V. Pavlyuk, A. Saccone, The isothermal section of the La-Ag-Mg phase diagram at 400 °C, Intermetallics. 19 (2011) 671–681. https://doi.org/10.1016/j.intermet.2011.01.007.
26. V. Kopský, D.B. Litvin, eds., International Tables for Crystallography, E (2010). https://doi.org/10.1107/97809553602060000109.